

Strain accumulation and rotation in western Nevada, 1993–2000

J. L. Svarc, J. C. Savage, and W. H. Prescott

U.S. Geological Survey, Menlo Park, California, USA

A. R. Ramelli

Nevada Bureau of Mines and Geology, University of Nevada, Reno, Nevada, USA

Received 18 May 2001; revised 28 October 2001; accepted 2 November 2001; published 9 May 2002.

[1] The positions of 44 GPS monuments in an array extending from the Sierra Nevada at the latitude of Reno to near Austin, Nevada, have been measured several times in the 1993–2000 interval. The western half of the array spans the Walker Lane belt, whereas the eastern half spans the central Nevada seismic zone (CNSZ). The principal strain rates in the Walker Lane belt are 29.6 ± 5.3 nstrain yr^{-1} N88.4°E $\pm 5.4^\circ$ and -12.8 ± 6.0 nanostrain yr^{-1} N01.6°W $\pm 5.4^\circ$, extension reckoned positive, and the clockwise (as seen from above the Earth) rotation rate about a vertical axis is 13.6 ± 4.0 nrad yr^{-1} . The quoted uncertainties are standard deviations. The motion in the Walker Lane belt can then be represented by a zone striking N35°W subject to 16.8 ± 4.9 nstrain yr^{-1} extension perpendicular to it and 19.5 ± 4.0 nstrain yr^{-1} right-lateral, simple shear across it. The N35°W strike of the zone is the same as the direction of the local tangent to the small circle drawn about the Pacific-North America pole of rotation. The principal strain rates for the CNSZ are 46.2 ± 11.0 nstrain yr^{-1} N49.9°W $\pm 6.0^\circ$ and -13.6 ± 6.1 nstrain yr^{-1} N40.1°E $\pm 6.0^\circ$, and the clockwise rotation rate about a vertical axis is 20.3 ± 6.3 nrad yr^{-1} . The motion across the CNSZ can then be represented by a zone striking N12°E subject to 32.6 ± 11.0 nstrain yr^{-1} extension perpendicular to it and 25.1 ± 6.3 nstrain yr^{-1} right-lateral, simple shear across it. The N12°E strike of the zone is similar to the strikes of the faults (Rainbow Mountain, Fairview Peak, and Dixie Valley) within it. **INDEX TERMS:** 1208 Geodesy and Gravity: Crustal movements— intraplate (8110); 8110 Tectonophysics: Continental tectonics—general (0905); **KEYWORDS:** Nevada, strain, rotation

1. Introduction

[2] Here we are concerned with deformation across the Walker Lane belt and the central Nevada seismic zone (CNSZ) between 39° and 40°N (Figure 1). Seismicity in the area is concentrated along the CNSZ and the western edge of the Walker Lane belt [Goter *et al.*, 1994]. The Walker Lane belt [Stewart, 1988] is a zone (width of ~ 100 km) of diverse topography intermediate between the typical Basin and Range topography (long chains of northerly trending mountain ranges separated by basins of comparable width) and the massive N30°W trending Sierra Nevada. The Walker Lane belt (Figure 1) is bounded on the northeast by the Walker Lane itself (a narrow linear zone passing near Fallon and Gabbs) and on the southwest by the Sierra Nevada front (roughly defined by a line trending N30°W through Lake Tahoe). Deformation in the Walker Lane belt between 39° and 40°N has been described in consecutive papers by Slemmons *et al.* [1979], Bell and Slemmons [1979], and Sanders and Slemmons [1979]. The CNSZ [Caskey *et al.*, 1996] is defined by the ruptures associated with the 1915 Pleasant Valley, 1954 Rainbow Mountain-Fairview Peak-Dixie Valley, and the 1932 Cedar Mountain earthquakes, all magnitude ~ 7 events [Goter *et al.*, 1994]. The Walker Lane belt and the CNSZ merge into the eastern California shear zone (ECSZ) at about 38°N. The ECSZ (site of the 1872 Owens Valley and 1992 Landers earthquakes [Goter *et al.*, 1994]) continues south to the east end of the Big Bend in the San Andreas fault. Roughly 25% of the Pacific-North American relative plate movement appears to be accommodated along the ECSZ, CNSZ, and Walker Lane belt.

Pezzopane and Weldon [1993] trace that relative motion farther north along faults in Oregon.

[3] To study the distribution of deformation across the Walker Lane belt and the CNSZ, the monuments within the geodetic array shown in Figure 1 were surveyed at least twice in the 1993–2000 interval using the Global Positioning System (GPS). The individual monuments in the array were occupied for at least 6 hours on each day, and the number of days occupied in each year is shown in Table 1. The data were reduced using point positioning [Zumberge *et al.*, 1997], GIPSY/OASIS II software, release 5 [Webb and Zumberge, 1995], and satellite and clock files from the Jet Propulsion Laboratory (JPL). The phase ambiguities in each survey were resolved in the network processing mode. The solutions were referred to International Terrestrial Reference Frame 1997 (ITRF97) (an update of ITRF96 [Sillard *et al.*, 1998]), but that solution was then rotated so that North America (NA) was nominally fixed using a NA-ITRF97 Euler vector (-2.20° N, 79.96° W, and 0.197° Myr $^{-1}$) similar to the NA-ITRF96 vector (-0.9° N, 79.8° W, and 0.192° Myr $^{-1}$) of Demets and Dixon [1999]. (The NA-ITRF97 Euler vector currently used by T. H. Dixon (personal communication, 2000) is -2.64° N, 79.12° W, and 0.199° Myr $^{-1}$.) Our Euler vector was determined so as to minimize the velocities at the ITRF97 fiducial stations Algo, Brmu, Chur, Drao, Gode, Kely, Mdo1, Nlib, Rcm5, Stjo, Thu1, Wes2, and Yell. Because it is not certain that all of those fiducial stations are, in fact, fixed with respect to NA, the velocities discussed here may have an additional common (systematic) uncertainty of perhaps 1 or 2 mm yr^{-1} . The relative velocities of the monuments within the array, however, are almost free of that systematic error.

[4] The standard deviation in a 1-day solution for each horizontal component of position of a monument relative to fixed NA is estimated to be ~ 4 mm. This estimate is based on data from

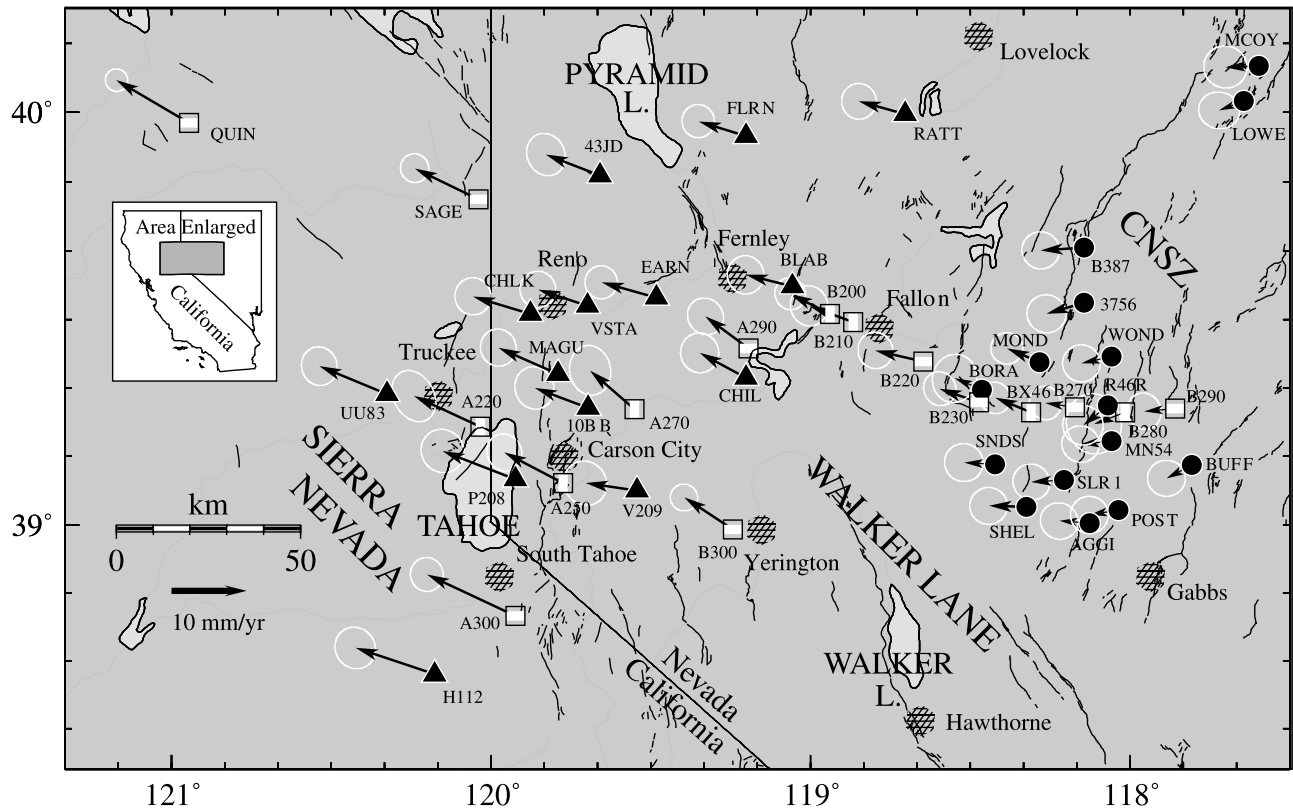


Figure 1. Map of western Nevada near Reno showing the locations of the GPS monuments in the western Nevada array. Open squares designate the Traverse subarray and the continuous GPS station Quin, solid triangles designate the Reno subarray, and solid circles designate the CNSZ subarray. The sinuous lines locate mapped active faults [Jennings, 1994]. Cities and towns are indicated by crosshatched circles. The velocities of the individual monuments relative to interior North America are indicated by arrows with a 95% confidence ellipse at the tip.

continuously recording GPS instruments in the San Francisco Bay area. There the formal error estimates from the GPS solutions must be increased by a factor 2 to account for the observed scatter about linear fits to the data. Average standard deviations derived by this scaling for the data for monuments Sage, B300, and Bx46 (data shown in Figure 2) are 3.3 mm in the north, 3.3 mm in the east, and 12.1 mm in the vertical. In sections 2 and 4 we demonstrate that these estimated standard deviations are appropriate. These estimated uncertainties do not include the systematic error in fixing the reference frame with respect to stable NA.

[5] The following conventions are observed in this paper: Uncertainties quoted in the text and tables are standard deviations, but error bars in the figures extend 2 standard deviations on either side of the plotted point. For strain rates, extension is reckoned positive, and tensor shear strain is used rather than engineering shear strain. Azimuths not bracketed by directions (e.g., N30°W) are measured clockwise from north. Rotation rates are reckoned positive in the counterclockwise direction as viewed from above the Earth. All velocities and rotations are measured relative to the fixed interior of NA.

2. Data

[6] The western Nevada GPS array shown in Figure 1 is a combination of three different arrays each surveyed at different times (Table 1). The Traverse subarray (open squares in Figure 1) of 15 monuments (A220, A250, A270, A290, A300, B200, B210, B220, B230, B270, B280, B290, B300, Bx46, and Sage) was surveyed by the U.S. Geological Survey (USGS) in 1992, 1996, 1998, and 2000. That subarray is part of a larger array that

extends across the entire Basin and Range province [Thatcher *et al.*, 1999], and the only addition here to the data of Thatcher *et al.* is the inclusion of the survey in 2000. The 14 monuments (solid triangles in Figure 1) 10bb, 43jd, Blab, Chil, Chlk, Earn, Flrn, H112, Magu, P208, Ratt, Uu83, V209, and Vsta, all west of 118.5°W, form the Reno subarray originally established by the University of Nevada in 1995 and resurveyed in 1996 and 2000 by the USGS. The CNSZ subarray (solid circles in Figure 1) of 15 monuments (3756, Aggi, B387, Bora, Buff, Mn54, Lowe, Mond, Post, R46r, Shel, Slr1, Snds, and Wond), all east of 118.5°W, is part of the geodetic array in the epicentral area of the 1954 Fairview Peak-Dixie Valley earthquakes, which was originally surveyed by the USGS with a Geodolite (an electro-optical distance measuring instrument) [Savage *et al.*, 1995]. We will be concerned here with the GPS surveys of those monuments by the USGS in 1994 and 2000. A summary of the monuments in each array, and the number of days in each year in which they were surveyed is given in Table 1. Detailed information on all monuments (latitude, longitude, elevation, times occupied, position versus time plots) can be found on a USGS Web site (<http://quake.wr.usgs.gov/docs/deformation/WesternNevada/>). The plots of observed positions of the individual monuments as a function of time shown on the Web site are simply the individual daily solutions referred to distant fiducial stations that represent the NA fixed reference frame. No attempt in the Web site has been made to combine those daily solutions to obtain consistency in the positions from day to day. Examples of these plots are shown in Figure 2 where the north, east, and up positions are plotted for the three monuments for which the most annual surveys were available. The measurements define

Table 1. Number of Days Monuments Were Occupied in Each Year

| Station | 1992 | 1994 | 1995 | 1996 | 1998 | 2000 |
|----------|------|------|------|------|------|------|
| Traverse | | | | | | |
| A220 | 1 | | | 1 | 1 | |
| A250 | 1 | | | 2 | 2 | 1 |
| A270 | 1 | | | 1 | 1 | |
| A290 | 1 | | | 1 | 1 | 1 |
| A300 | 1 | | | 2 | 2 | |
| B200 | 3 | | | 4 | 4 | 1 |
| B210 | 1 | | | 1 | 1 | 1 |
| B220 | 1 | | | 1 | 1 | 1 |
| B230 | 1 | | | 1 | 1 | 2 |
| B270 | 1 | | | 1 | 1 | 2 |
| B280 | | | | 1 | 1 | 1 |
| B290 | 1 | | | 1 | 1 | 2 |
| B300 | 3 | | 3 | 6 | 3 | 4 |
| Bx46 | 2 | 1 | | 2 | 2 | 2 |
| Sage | 1 | | 2 | 4 | 2 | 3 |
| Reno | | | | | | |
| 10bb | | | 2 | 3 | | 2 |
| 43jd | | | 2 | 2 | | 2 |
| Blab | | | 2 | 2 | | 2 |
| Chlk | | | 1 | 2 | | 3 |
| Earn | | | 2 | 8 | | 2 |
| Flrn | | | 2 | 2 | | 3 |
| H112 | | | 2 | 2 | | 2 |
| Magu | | | 2 | 3 | | 2 |
| P208 | | | 2 | 3 | 1 | 2 |
| Ratt | | | | 3 | 4 | 3 |
| Uu83 | | | 4 | 4 | 2 | 2 |
| V209 | | | 2 | 2 | | 2 |
| Vsta | | | 2 | 2 | | 2 |
| CNSZ | | | | | | |
| 3756 | | 1 | | | | 2 |
| Aggi | | 1 | | | | 3 |
| B387 | | 2 | | | | 2 |
| Bora | | 1 | | | | 2 |
| Buff | | 1 | | | | 2 |
| Lowe | | 1 | | | | 2 |
| Mcoy | | 1 | | | | 3 |
| Mn54 | | 1 | | | | 3 |
| Mond | | 2 | | | | 2 |
| Post | | 1 | | | | 2 |
| R46r | | 1 | | | | 2 |
| Shel | | 1 | | | | 2 |
| Slr1 | | 1 | | | | 2 |
| Snds | | 1 | | | | 1 |
| Wond | | 1 | | | | 2 |

linear trends, suggesting that the motion has been uniform in time. The residuals of the observations from the linear trends are consistent with the a priori estimates of standard deviation (i.e., twice the formal error in the solution).

[7] We have used the adjustment program QOCA [Dong *et al.*, 1998] (see also the Web site <http://sideshow.jpl.nasa.gov:80/~dong/qoca/>) in the global mode to find the velocity at each monument. That adjustment program combines the loosely constrained daily solutions by subjecting each to a Helmert transformation (adjust rotation, dilatation, and translation) such that the solutions are as consistent as possible with deformation that is linear in time. We included in the QOCA the adjustment GPS station Quin (Figure 1), which is operated continuously (solutions available every day) by JPL. (The inferred velocities with standard deviations are shown on the Web site <http://quake.wr.usgs.gov/docs/deformation/Western-Nevada/>.) The average standard deviation in both the north and east components of velocity is $\sim 1.0 \text{ mm yr}^{-1}$. That estimate of standard deviation includes an arbitrary allowance ($1 \text{ mm } \sqrt{\text{yr}^{-1}}$ random walk) for instability at each monument.

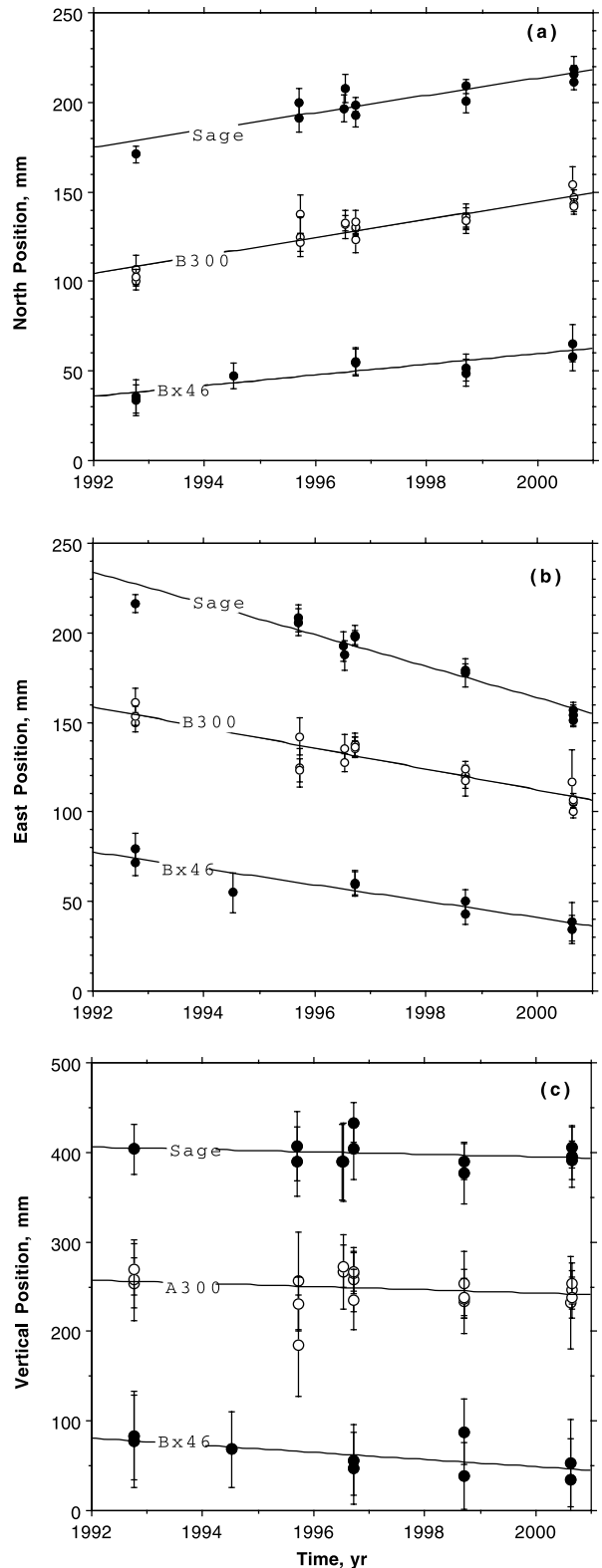


Figure 2. Daily positions plotted as a function of time for the three monuments with the most complete observations. (a) North component, (b) east component, and (c) uplift. The error bars represent two standard deviations on either side of the plotted point.

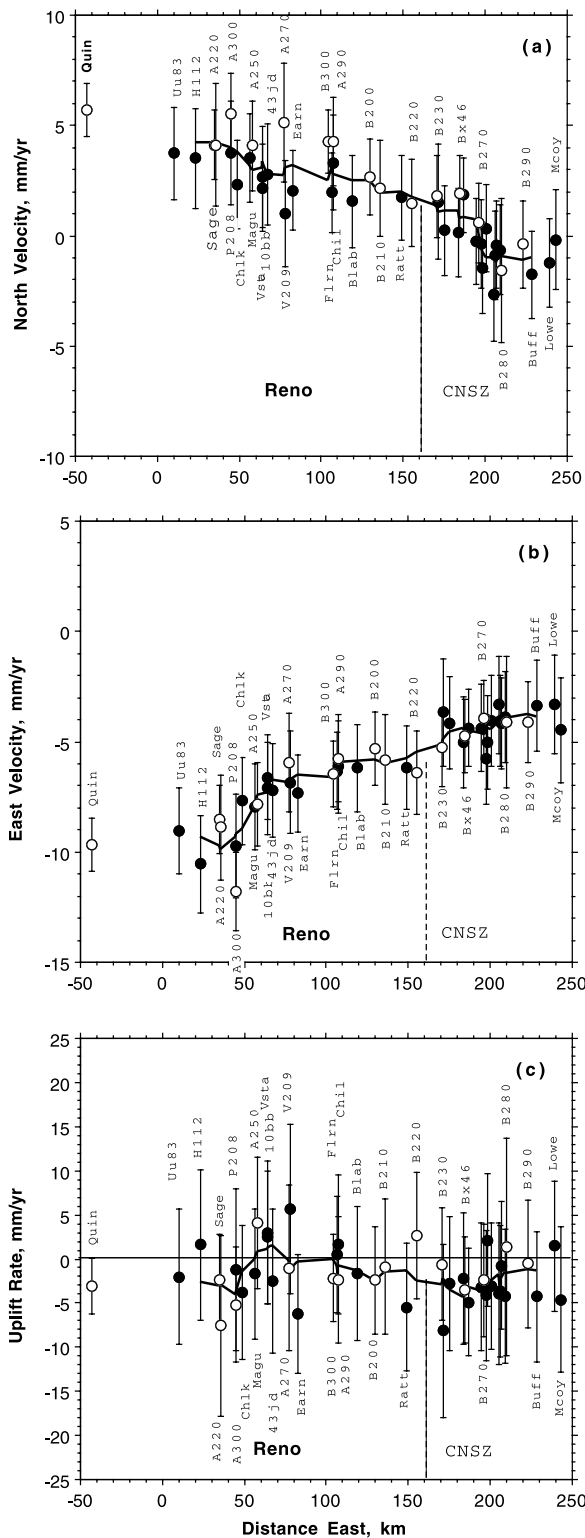


Figure 3. Velocities measured at each monument plotted as a function of the distance east of a point 10 km west of monument Uu83. Monuments in the Traverse subarray and Quin are identified by open circles, monuments in the Reno subarray are shown by the solid circles to the left of the vertical line near abscissa 160 km, and monuments in the CNSZ subarray are shown by the solid circles to the right of that line. (a) North velocity, (b) east velocity, and (c) uplift rate. The error bars represent 2 standard deviations on either side of the plotted points. Also shown in each plot (solid sinuous line) is a five-point running average of the data.

3. Velocity Profiles

[8] The average 1993–2000 velocities relative to fixed interior NA inferred from the QOCA adjustment are shown in Figure 1. The velocity vectors at the west end of the array are directed ($N60^{\circ}W \pm 3.1^{\circ}$, $N64^{\circ}W \pm 4.7^{\circ}$, and $N65^{\circ}W \pm 6.5^{\circ}$ for monuments Quin, Sage, and A300, respectively) somewhat more westerly than the tangent (strike $N49^{\circ}W$) to the local small circle drawn about the Sierra Nevada-NA pole [Dixon *et al.*, 2000]. Figure 3 shows a profile of the north and east velocity components as a function of the distance east from a point 10 km west of monument Uu83. The trend in those plots is indicated by the sinuous line, which connects the smoothed velocities (each velocity replaced by the average of five velocities, that velocity itself and the velocities of the two closest monuments on both sides). The uplift rate plot in Figure 3c is included only for completeness; we are not at present sufficiently confident of our measurements of uplift to attach significance to the small signal shown.

[9] Three monuments, H112, P208, and A300, have east velocities that fall noticeably below the trend in Figure 3b. Those monuments are the only ones located on the western block of the Genoa fault (fault running south from Carson City in Figure 1). It is possible that the anomalous westward motion of those monuments is associated with strain accumulation on that fault.

[10] The horizontal velocities at the east end of the profiles in Figure 3 are about -4 mm yr^{-1} east and -1 mm yr^{-1} north relative to fixed NA. Because there are no obvious tectonic elements east of $118^{\circ}W$ which would contribute a southward velocity, we believe that the north velocity should not be less than 0. We suspect that the negative velocity found reflects the uncertainty in referring our velocities to fixed NA. The -4 mm yr^{-1} eastward velocity is attributed to east-west extension of the Basin and Range province east of $118^{\circ}W$. Much of that westward velocity may be contributed by strain accumulation on the Wasatch fault at the east edge of the Basin and Range province [Thatcher *et al.*, 1999].

[11] Figure 4 shows a more detailed plot of the portion of Figure 3 that crosses the 1954 Fairview Peak-Dixie Valley rupture (location approximated by the dashed vertical line in Figure 4). Figure 4a suggests a significant right-lateral offset near the rupture. The offset appears to be confined to within a zone of perhaps $\sim 10\text{-km}$ width. Postseismic creep ($\sim 2 \text{ mm yr}^{-1}$) on the rupture is not excluded by the observations. In contrast, the eastward velocity (Figure 4b) across the Fairview Peak-Dixie Valley indicates broadly distributed east-west extension with no significant anomaly near the rupture crossing.

4. Strain Rates

[12] The regional motion of a small geodetic array (aperture a few degrees in latitude and longitude) can be approximated by the combination of a rigid-body motion of the array as a whole plus a uniform strain rate within the network. Such an approximation is included in the QOCA program, but here we use the formulation in spherical coordinates by Savage *et al.* [2001, Appendix]. The strain and rotation rates found from such an analysis are shown in Table 2 for the entire Western Nevada array and for several subarrays. Station Quin, which lies somewhat outside the area of interest, was not included in the strain calculations. The strain rates ϵ_{11} , ϵ_{12} , and ϵ_{22} in Table 2 are referred to a geographic coordinate system (1 axis directed east and 2 axis north); ϵ_1 and ϵ_2 are the principal strain rates; and the azimuth of ϵ_2 (greatest contraction rate) is measured clockwise from north. The counterclockwise (as viewed from above the Earth) rotation rate ω_r about the vertical axis through the centroid of the subarray is shown in Table 2. Also shown in Table 2 is the standard deviation of an observation of unit weight [Bomford, 1971, p. 621]. That standard deviation should be 1 if the standard deviations of the observations are appropriate and the model (rigid-body motion plus uniform strain) fits the observed

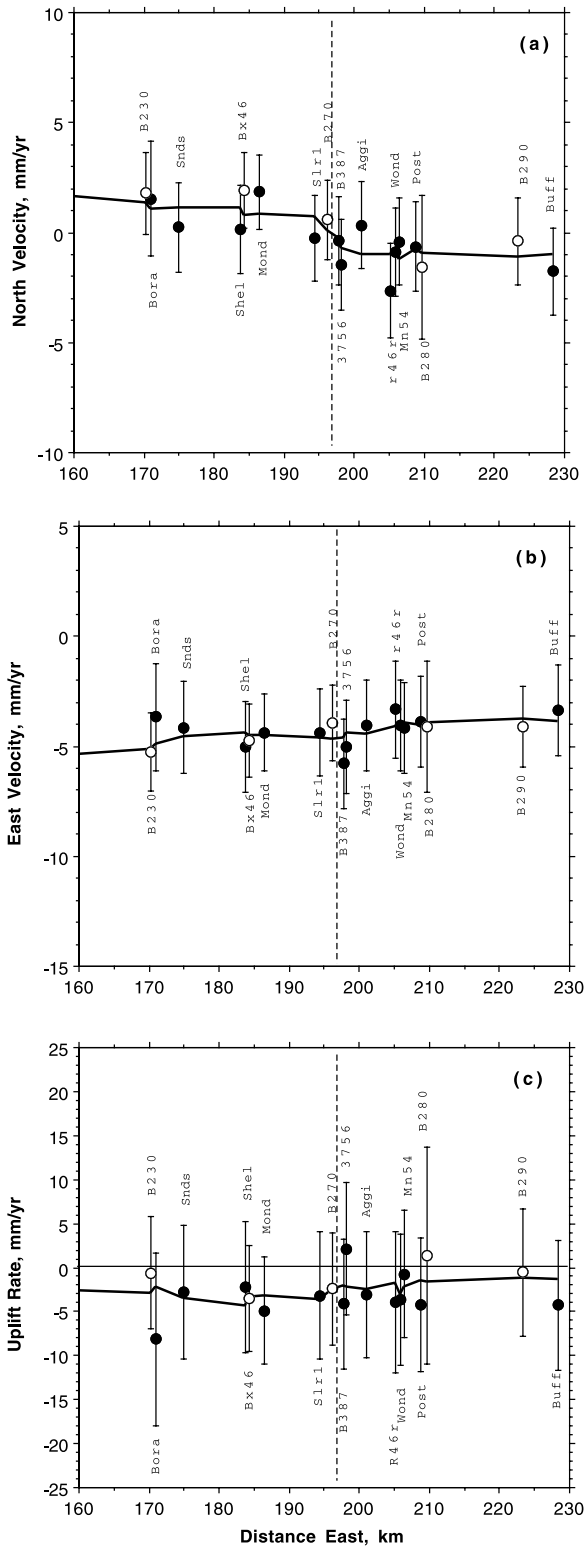


Figure 4. Detailed plot of the data between abscissa 160 and 230 km in Figure 3. That distance interval spans the 1954 Rainbow Mountain-Fairview Peak-Dixie Valley rupture. Monuments in the Traverse subarray are identified by open circles, and monuments in the CNSZ subarray are shown by the solid circles. The dashed vertical line separates monuments (left) on the western fault block from those (right) on the eastern block. (a) North velocity, (b) east velocity, and (c) uplift rate. The error bars represent 2 standard deviations on either side of the plotted points. Also shown in each plot (solid sinuous line) is a five-point running average of the data.

motion. As can be seen in Table 2, the standard deviation of an observation of unit weight is close to 1 for all subarrays except for the northern Basin and Range (NBAR) entries in Table 2. (The NBAR array will be discussed in section 6.) Thus the standard deviations ($\sim 1 \text{ mm yr}^{-1}$) estimated for the velocities in the western Nevada array appear to be reasonable.

[13] The strain and rotation rates for the entire western Nevada array, which includes 44 of the monuments in Figure 1 (continuous GPS station Quin excluded), is shown in Table 2. That array is made up of three subarrays, CNSZ, Reno, and Traverse (Table 1), and the strain and rotation rates for those three subarrays individually are shown in Table 2. The shear strain rate ϵ_{12} for the CNSZ subarray seems anomalous with respect to the other subarrays; we attribute this to the concentrated right-lateral shear across the 1954 rupture (Figure 4a).

[14] The western Nevada array has been divided into two subarrays at longitude 118.5°W (Figure 1), the 20-monument East Half subarray east of 118.5°W and the 24 monument West Half subarray west of 118.5°W . The dividing longitude was chosen so that the East Half subarray contains all monuments likely to have been significantly affected by the 1954 earthquakes.

[15] The strain and rotation rates for the entire West Half subarray are shown in Table 2, and in Traverse subarray monuments and Reno subarray monuments entries the West Half subarray is broken down according to surveyed subarrays (Traverse and Reno, respectively). The strain and rotation rates for the Walker Lane belt are given, the West Half array without monument Ratt. The strain rates for these four subarrays (Table 2) are reasonably consistent with one another. We will be most interested in the Walker Lane belt (Table 2) as it spans the transition from the Basin and Range province to the Sierra Nevada.

[16] The strain and rotation rates for the East Half subarray, which includes the entire CNSZ subarray and monuments B230, B270, B280, B290, and Bx46 from the Traverse subarray, are shown in Table 2. As argued above, strain accumulation in the East Half subarray is not homogeneous because it includes the concentrated shear along the 1954 Fairview Peak-Dixie Valley rupture (Figure 4a). To eliminate that concentrated shear from our calculations, we have calculated shear strain and rotation rates for the monuments on the fault blocks (Table 2) on either side of the 1954 rupture in the East Half subarray. The strain and rotation rates for the East block are consistent with those found for the Walker Lane belt, but the strain rate ϵ_{22} for the West block is significantly larger than that found for the Walker Lane belt.

[17] The southeasternmost 16 monuments (Aggi, B230, B270, B280, B290, Bx46, Bora, Buff, Mn54, Mond, Post, R46r, Shel, Slr1, Snds, and Wond) of the western Nevada array cover the same area as the Fairview geodetic array measured by Geodolite between 1973 and 1994 [Savage *et al.*, 1995, Figure 2]. Indeed, monuments Bx46, Bora, Buff, Mn54, Mond, Post, R46r, Shel, Slr1, Snds, and Wond in the CNSZ subarray are part of the Fairview geodetic array. The principal strain rates for this area measured by GPS over the interval 1994–2000 (Table 2) can be compared to those ($\epsilon_{11} = 16 \pm 10 \text{ nstrain yr}^{-1}$, $\epsilon_{12} = -32 \pm 5 \text{ nstrain yr}^{-1}$, and $\epsilon_{22} = -25 \pm 9 \text{ nstrain yr}^{-1}$) measured by Geodolite over the interval 1973–1994 [Savage *et al.*, 1995, Table 1]. The measured values of ϵ_{11} and ϵ_{12} are in good agreement, but the values for the north-south extension ϵ_{22} differ by a marginally significant amount ($41 \pm 16 \text{ nstrain yr}^{-1}$). The Geodolite strain determination was compromised by the loss of the central station Fairview in the middle of the time interval spanned, and we prefer the GPS strain measurement.

5. Rotation Rates

[18] The motion of a geodetic array has been approximated by a uniform strain rate within the array and a rigid-body motion of the

Table 2. Strain, Principal Strain, and Rotation Rates With Standard Deviations

| Array | ϵ_{11}^a , nstrain yr ⁻¹ | ϵ_{12}^a , nstrain yr ⁻¹ | ϵ_{22}^a , nstrain yr ⁻¹ | ϵ_1 nstrain yr ⁻¹ | ϵ_2 nstrain yr ⁻¹ | Contraction Azimuth, deg | ω_r , nrad yr ⁻¹ | σ |
|--------------------------------|---|---|---|--|--|--------------------------------|---------------------------------------|----------|
| Western Nevada | 26.1 ± 2.2 | -10.5 ± 2.4 | -3.4 ± 4.3 | 29.4 ± 2.6 | -6.7 ± 4.1 | 17.7 ± 3.9 | -15.1 ± 2.4 | 1.00 |
| CNSZ | 20.2 ± 13.7 | -25.7 ± 7.8 | 10.1 ± 7.5 | 41.3 ± 13.9 | -11.0 ± 7.0 | 39.5 ± 8.6 | -16.7 ± 7.8 | 0.83 |
| Reno | 20.6 ± 6.8 | -1.9 ± 4.9 | -1.8 ± 7.0 | 20.8 ± 7.2 | -2.0 ± 6.6 | 4.9 ± 12.4 | -12.5 ± 4.9 | 0.70 |
| Traverse | 28.6 ± 3.8 | -4.1 ± 4.5 | -13.6 ± 8.4 | 29.0 ± 3.8 | -13.9 ± 8.3 | 5.5 ± 6.1 | -23.3 ± 4.6 | 0.96 |
| West Half ^b | 26.9 ± 5.3 | -0.2 ± 3.9 | -12.4 ± 5.8 | 26.9 ± 5.3 | -12.4 ± 5.8 | 0.3 ± 5.7 | -11.9 ± 3.9 | 1.00 |
| Traverse | 33.0 ± 7.8 | -1.5 ± 6.3 | -14.2 ± 9.7 | 33.1 ± 7.8 | -14.3 ± 9.7 | 1.8 ± 7.6 | -20.0 ± 6.3 | 1.11 |
| Reno | 20.6 ± 6.8 | -1.9 ± 4.9 | -1.8 ± 7.0 | 20.8 ± 7.2 | -2.0 ± 6.6 | 4.9 ± 12.4 | -12.5 ± 4.9 | 0.70 |
| Walker Lane belt ^c | 29.6 ± 5.4 | 1.2 ± 4.0 | -12.8 ± 5.9 | 29.6 ± 5.3 | -12.8 ± 6.0 | -1.6 ± 5.4 | -13.6 ± 4.0 | 0.98 |
| East Half ^d | 21.4 ± 10.5 | -29.5 ± 6.3 | 11.2 ± 6.8 | 46.2 ± 11.0 | -13.6 ± 6.1 | 40.1 ± 6.0 | -20.3 ± 6.3 | 0.80 |
| East block ^e | 38.1 ± 17.1 | -8.5 ± 9.1 | 0.2 ± 6.8 | 39.9 ± 17.6 | -1.7 ± 5.5 | 12.1 ± 12.5 | 5.1 ± 9.1 | 0.71 |
| West block ^f | 20.9 ± 20.7 | -10.6 ± 13.1 | 54.3 ± 15.0 | 57.4 ± 15.2 | 17.8 ± 20.7 | 73.7 ± 18.9 | -20.0 ± 13.1 | 0.55 |
| Fairview ^g | 19.7 ± 11.0 | -27.4 ± 8.8 | 16.3 ± 13.4 | 45.4 ± 11.5 | -9.5 ± 13.1 | 43.2 ± 9.0 | -29.7 ± 8.8 | 0.73 |
| NBAR west of Lewi ^h | 12.5 ± 3.6 | 2.7 ± 3.6 | -14.3 ± 6.3 | 12.8 ± 3.7 | -14.5 ± 6.3 | -5.7 ± 7.6 | -21.2 ± 3.6 | 4.56 |
| Without Slid | 8.8 ± 2.0 | -5.2 ± 2.4 | -18.8 ± 4.2 | 9.7 ± 1.8 | -19.8 ± 4.2 | 10.3 ± 4.6 | -13.9 ± 2.4 | 2.28 |
| NBAR east of Lewi ⁱ | 8.2 ± 0.9 | 1.5 ± 1.0 | 0.0 ± 1.7 | 8.5 ± 1.0 | -0.2 ± 1.6 | -10.2 ± 6.3 | -1.5 ± 1.0 | 2.63 |

^aThe 1 axis is directed east and the 2 axis is directed north.

^bThe 24 monuments in the western Nevada array west of 118.5°W.

^cSame as West Half but without Ratt.

^dThe 20 monuments in the western Nevada array east of 118.5°W.

^eSites 3756, Aggi, B280, B290, B387, Buff, Lowe, Mcoy, Mn54, Post, R46r, and Wond.

^fB230, B270, Bx46, Bora, Mond, Shel, Slr1, and Snds.

^gAggi, B230, B270, B280, B290, Bx46, Bora, Buff, Mn54, Mond, Post, R46r, Shel, Slr1, Snds, and Wond.

^hQuin, Shin, Slid, Garl, Upsa, Tung, and Newp [Wernicke et al., 2000].

ⁱMine, Elko, Ruby, Egan, Gosh, Foot, Ceda, Smel, Coon, Hebe, and Cast [Wernicke et al., 2000].

array as a whole. As is familiar from plate tectonics, horizontal rigid-body motion on a sphere is simply a rotation about an axis through the center of the sphere. The Euler vectors that describe the rotation for the various subarrays are shown in Table 3. The position of the poles for the entire western Nevada array and the east and west halves of that array are shown in Figure 5. The poles for the other subarrays are generally distributed along the north-northeast trend defined by those three poles. The rotation poles are only a few degrees distant in latitude and longitude from the associated subarrays, and the total rotation rate (Table 3) is very nearly equal to the radial component ω_r (Table 2) (i.e., the other two components ω_ϕ and ω_θ of the rotation rate are small). None of the rotation poles in Table 3 corresponds to the Pacific-NA pole (50.5°N, 75.8°W [Demets and Dixon, 1999]) or the Sierra Nevada-NA pole (17.1°N, 137.8°W [Dixon et al., 2000]). Such a correspondence might have been expected if the observed motion were simply a distributed response in the NA plate to relative plate rotation, i.e., if the western part of the NA plate were not rigid but rather underwent internal deformation in response to the plate-driving forces. The pole of rotation for the entire western Nevada network (Table 3) is located (Figure 5) in southeastern Oregon ~170 km east-southeast of the pole of rotation found for western Oregon and southwestern Washington (Euler vector 43.40°N ± 0.14°, 119.33°W ± 0.28°, and -0.822 ± 0.057° Myr⁻¹ [Svarc et al., 2002]). Although the 95% confidence ellipses for the poles of rotation of the Euler vectors for the western Nevada network (Table 2) and for western Oregon and southwestern Washington do not overlap, the similarity of the Euler vectors does suggest a possible common rigid body rotation combined with internal deformation that is not adequately described by uniform strain. However, the fact that the Euler vectors for the various subarrays in Table 3 are not closely similar suggests that the Nevada data are not readily interpreted as the rigid rotation of a microplate. That is, we believe that the Euler vectors in Table 3 simply define the motion of the centroid of each subarray and that those Euler vectors should not be interpreted in terms of rigid block motion of individual subarrays.

[19] On the basis of paleomagnetic rotations in the Walker Lane belt north of 39°N, Cashman and Fontaine [2000] concluded that

north of 40°N, right-lateral shear across the Walker Lane belt is accommodated by strike slip on northwest striking faults (e.g., Pyramid Lake fault) with no accompanying paleomagnetic rotation. Slip on these faults should release both the strain and rotation accumulation so that no secular block rotation is expected. In contrast, within the region between 39°N and 40°N, Cashman and Fontaine observed secular clockwise rotation at a rate greater than about 4.0 ± 0.5° Myr⁻¹ and suggest that right-lateral simple shear across the Walker Lane belt in this region is accommodated by left-lateral slip on northeast striking faults (Olinghouse fault, Carson lineament, and Wabuska lineament) plus clockwise rotation. (These paleomagnetic rotations are measured relative to the Sierra Nevada block [Cashman and Fontaine, 2000, p. 120], but the 0.28° Myr⁻¹ rotation of the Sierra Nevada block relative to fixed NA [Dixon et al., 2000] is sufficiently small that the rotations may be treated as if measured with respect to fixed NA.) Such rotation is required to convert left-lateral simple shear across the northeast striking faults to right-lateral simple shear across the Walker Lane belt (see Appendix A). That is, right-lateral simple shear is accumulating across the Walker Lane belt between 39°N and 40°N just as it is farther north, and the interseismic strain and rotation rates observed should be comparable in the two areas. However, between 39°N and 40°N that motion is accommodated primarily by left-lateral slip on northeast striking faults rather than by right-lateral slip on northwest striking faults. In either case, the shear strain will be released, but right-lateral slip on northwest striking faults will release accumulated rotation, whereas left-lateral slip on northeast striking faults will augment the accumulated rotation. Thus the geodetically measured interseismic rotation rate between 39°N and 40°N should be equal to ϵ_{12} , but the secular (paleomagnetic) rotation rate should be $2\epsilon_{12}$. The model is qualitatively consistent with our geodetic observations, but the minimum inferred paleomagnetic rotation rate (-4.0 ± 0.5° Myr⁻¹) is significantly greater than twice the geodetic rotation rate (-0.8° Myr⁻¹, Table 3).

[20] We use the rotation component ω_r in Table 2 principally to identify simple shear (see Appendix A). For example, for western Nevada in Table 2 the fact that the rotation ω_r is approximately equal to the shear strain rate ϵ_{12} implies that the motion is

Table 3. Euler Vector for Subarrays

| Array | Array Latitude, °N | Array Longitude, °W | Pole Latitude, °N | Pole Longitude, °W | Ω , deg Myr ⁻¹ |
|--------------------------------|--------------------|---------------------|-------------------|--------------------|----------------------------------|
| Western Nevada | 39.36 | 118.88 | 42.92 ± 0.57 | 117.48 ± 0.26 | -0.87 ± 0.14 |
| CNSZ | 39.36 | 118.09 | 41.67 ± 1.07 | 118.34 ± 0.20 | -0.96 ± 0.45 |
| Reno | 39.44 | 119.60 | 44.79 ± 2.06 | 116.99 ± 1.12 | -0.72 ± 0.28 |
| Traverse | 39.29 | 119.00 | 41.75 ± 0.48 | 117.54 ± 0.32 | -1.34 ± 0.26 |
| West Half ^a | 39.38 | 119.52 | 44.96 ± 1.81 | 116.15 ± 1.22 | -0.68 ± 0.22 |
| Traverse | 39.30 | 119.42 | 42.58 ± 1.02 | 117.09 ± 0.79 | -1.15 ± 0.36 |
| Reno | 39.44 | 119.60 | 44.79 ± 2.06 | 117.00 ± 1.12 | -0.72 ± 0.28 |
| Walker Lane belt ^b | 39.35 | 119.56 | 44.28 ± 1.43 | 116.59 ± 0.95 | -0.78 ± 0.23 |
| East Half ^c | 39.34 | 118.11 | 41.27 ± 0.60 | 118.15 ± 0.11 | -1.16 ± 0.36 |
| East block ^d | 39.45 | 117.95 | 32.15 ± 12.67 | 116.15 ± 2.95 | -0.30 ± 0.51 |
| West block ^e | 39.21 | 118.31 | 41.29 ± 1.33 | 117.71 ± 0.42 | -1.14 ± 0.75 |
| Fairview ^f | 39.22 | 118.17 | 40.52 ± 0.38 | 118.11 ± 0.07 | -1.70 ± 0.50 |
| NBAR west of Lewi ^g | 40.02 | 119.28 | 42.76 ± 0.43 | 116.73 ± 0.49 | -1.22 ± 0.21 |
| Without Slid | 40.12 | 119.18 | 43.76 ± 0.58 | 115.43 ± 0.70 | -0.80 ± 0.14 |
| NBAR east of Lewi ^h | 40.14 | 113.62 | 53.82 ± 8.31 | 106.46 ± 5.81 | -0.09 ± 0.05 |

^a The 24 monuments in the Western Nevada array west of 118.5°W.

^b Same as West Half but without Ratt.

^c The 20 monuments in the Western Nevada array east of 118.5°W.

^d The sites 3756, Aggi, B280, B290, B387, Buff, Lowe, Mcoy, Mn54, Post, R46r, and Wond.

^e B230, B270, Bx46, Bora, Mond, Shel, Slr1, and Snds.

^f Aggi, B230, B270, B280, B290, Bx46, Bora, Buff, Mn54, Mond, Post, R46r, Shel, Slr1, Snds, and Wond.

^g Quin, Shin, Slid, Garl, Upsa, Tung, and Newp [Wernicke *et al.*, 2000].

^h Mine, Elko, Ruby, Egan, Gosh, Foot, Ceda, Smel, Coon, Hebe, and Cast [Wernicke *et al.*, 2000].

approximately that associated with right-lateral, simple shear across (see Appendix), and extension (ϵ_{11}) perpendicular to, a north striking zone. Such simple shear and extension are readily associated with strain accumulation on a north striking right-

oblique, normal fault. The rotation detected here then may be part of the strain accumulation cycle, in which case most of it would be released with the accumulated right-lateral strain in subsequent earthquakes. We will discuss this interpretation further in section 7. The fact that all the subarrays in Table 2 (except East block and NBAR east of Lewi) exhibit essentially the same value of ω_r suggests a regional phenomenon. The exceptional value of ω_r for East block of Table 2 is readily explained: Recall that in treating the East and West blocks of the East Half array independently, we have excluded the zone of simple shear along the 1954 Fairview Peak-Dixie Valley rupture zone (Figure 4a) where the rotation would be concentrated. Thus small rotation rates for those blocks might have been expected. The NBAR east of Lewi entry in Table 2 represents a region well east of that discussed here.

6. Velocity Profiles Across the Entire Basin and Range

[21] The Traverse subarray (open squares in Figure 1) discussed in this paper is the western portion of the array used by Thatcher *et al.* [1999] to measure deformation between 39°N and 40°N across the entire Basin and Range province. We have simply added a survey in 2000 to the data from their surveys in 1992, 1996, and 1998. Thus the strain and rotation rates for the western part of the array surveyed by Thatcher *et al.* [1999] are given for Traverse in Table 2.

[22] Wernicke *et al.* [2000] inferred average velocities between 1996 and 1999 from continuously operated (i.e., daily solutions available) GPS stations in their northern Basin and Range (NBAR) array, an array which can roughly be described as two parallel profiles across the Basin and Range province at latitude $\sim 40^\circ$ N. Station Quin (Figure 1) is the westernmost of those stations. The velocities found by Wernicke *et al.* [2000] are given on their Web site (http://cfa-www.harvard.edu/space_geodesy/BARGEN/Wernicke/2000_GSA_Velocity_Table.html). The velocity they assign to Quin (7.51 ± 0.16 mm yr⁻¹ north and 7.41 ± 0.16 mm yr⁻¹ west) differs by almost 3 mm yr⁻¹ from the value we found (5.69 ± 0.61 mm yr⁻¹ north and 9.67 ± 0.61 mm yr⁻¹ west). The difference may be in part due to differences in the NA fixed reference frames to which the velocities are referred and possibly also to the different time intervals considered (1996–1999 by Wernicke *et*

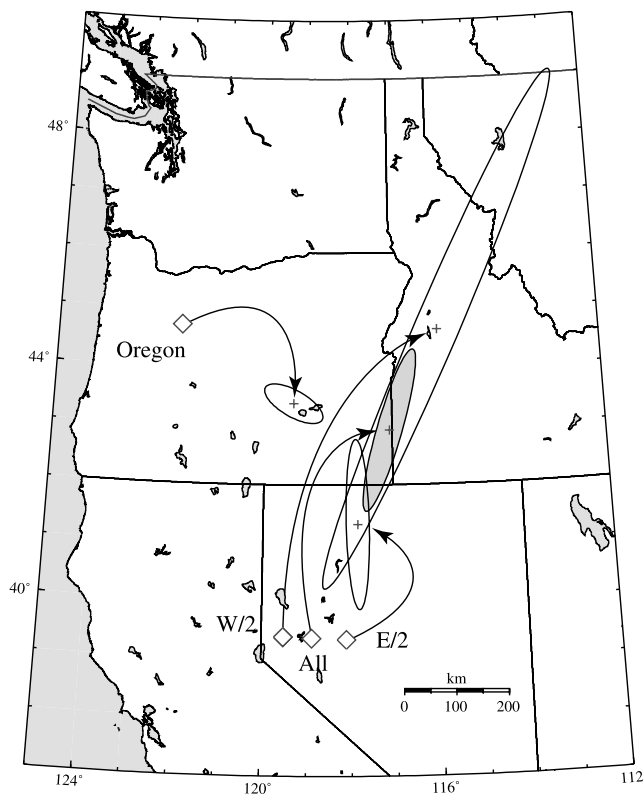


Figure 5. Map of northwestern United States showing the location of the poles of rotation (with 95% confidence ellipses) for the entire western Nevada subarray (All), and the west (W/2) and east (E/2) halves (see Table 3). Also shown is the pole for the rotation of western Oregon [Svarc *et al.*, 2002].

al., whereas we considered 1992–2000). In any case, the discrepancy is larger than expected.

[23] We have used the velocities measured by *Wernicke et al.* [2000] to calculate strain and rotation rates for the portions of their array west of 117.5°W (NBAR west of Lewi in Tables 2 and 3) and east of 116.5°W (NBAR east of Lewi in Tables 2 and 3). (Because the velocity measured at station Lewi in their array appears anomalous, that station was not included in either of the subarrays considered here.) The velocity measured at station Slid also appears anomalous, and thus strain and rotation rates for the subarray NBAR west of Lewi are shown with and without Slid (Tables 2 and 3). Notice that the standard deviation of an observation of unit weight for the NBAR entries in Table 2 indicates that either the standard deviations (~ 0.18 mm yr⁻¹) assigned to the velocity components on the Web site are too small or that the observed deformation in the subarray is not well described by the simple model of rigid block motion plus uniform strain rate. Because in their discussion *Wernicke et al.* [2000, p. 5] claim only a standard deviation in the measured velocity components of 0.5 mm yr⁻¹ (with a proviso that it may be as low as 0.1–0.2 mm yr⁻¹), we assume here that the standard deviations on the Web site are too small by a factor $0.5/0.18 = 2.8$, a factor consistent with the standard deviation of an observation of unit weight found in Table 2. The standard deviations for the strain and rotation rates quoted in Table 2 are determined by the weighted fit to the data and are not changed by this increase in the standard deviation of the NBAR observations.

[24] The strain and rotation rates for the subarray NBAR west of Lewi without Slid (Table 2) can be compared to our result for western Nevada (Table 2). Whereas our strain measurement is nearly a N72°W uniaxial extension, their strain rate is more nearly a N10°E uniaxial contraction. The only significant difference between the two is an isotropic extension rate of 16 nstrain yr⁻¹. That is, both shear components ($2\varepsilon_{12}$ and $\varepsilon_{11} - \varepsilon_{22}$) and the rotation components ω_r agree quite well, but the dilatation rates ($\varepsilon_{11} + \varepsilon_{22}$) differ by 32.7 ± 6.7 nstrain yr⁻¹. We do not understand why that difference in the deformation of the two arrays should appear only in the dilatation rate. Because the NBAR array overlaps the north edge of our western Nevada array, we had expected the strain and rotation rates in the two arrays to be similar. We noted earlier (section 3) that the east velocity of the three southwesternmost monuments in Figure 1 appear to be low (Figure 3b) relative to the trend of the other data. That also appears to be true for the southwesternmost station (Slid) in the NBAR array relative to the trend of the other NBAR data.

[25] The strain and rotation rates for the subarray NBAR east of Lewi (Table 2) indicate that Nevada east of the CNSZ is subject to uniform N79.8°W $\pm 6.3^\circ$ extension at the rate of 8.5 ± 2.8 nstrain yr⁻¹ and no significant rotation. That extension is perpendicular to the trend of the mountain ranges in the northern Basin and Range province.

7. Discussion

7.1. Stress Field in Western Nevada

[26] The stress field in western Nevada probably arises from two sources [*Flesch et al.*, 2000]: (1) the boundary stresses associated with motion of the Pacific plate relative to NA and (2) the buoyancy stress associated with gravity acting upon neighboring elevation differences [*Jones et al.*, 1996]. The former stress is approximately a right-lateral, simple shear (i.e., N80°W deviatoric tension and N10°E deviatoric compression) across the local tangent (strike about N35°W) to the small circle drawn about the Pacific-NA pole [*Demets and Dixon*, 1999]. The buoyancy stress is associated with the difference in elevation between the southwestern continental United States and the neighboring seafloor of the Pacific Ocean. Clearly, the gravitational potential energy (GPE) of the Earth [*Jones et al.*, 1996] could be reduced if a highstanding continent could

spread out in the same manner as a floating ice shelf spreads to reduce its potential energy [*Weertman*, 1957]. In western Nevada one might expect the buoyancy stress to be a uniaxial deviatoric tension directed normal (S55°W) to the local small circle drawn about the Pacific-NA pole (i.e., normal to the transform plate boundary which separates the high interior continent from the low Pacific basin). Although the relative strengths of the two stress fields is not assessed, the resultant stress field should involve principal tension in a direction intermediate between N80°W (from the boundary stress) and S55°W (from the buoyancy stress).

[27] *Flesch et al.* [2000] have evaluated the stresses induced by gravity and boundary forces more completely. Their calculation is based on the thin viscous sheet model of the lithosphere [*England and Jackson*, 1989]. Specifically, *Flesch et al.* [2000, Figure 2a] derive from the GPE distribution the deviatoric stress field for the southwestern United States subject to the constraint that the root-mean-square stress deviator be a minimum. This is a particular solution in which no explicit boundary condition has been imposed at the plate edge. They find that this GPE solution subjects most of Nevada to a north to north-northeast uniaxial deviatoric tension. (The fact that the tension is not perpendicular to the plate boundary is apparently due to the east-northeast trending ridge of high GPE across central Nevada [*Flesch et al.*, 2000, Figure 2a], which produces spreading perpendicular to trend.) In addition to the GPE-induced stresses, *Flesch et al.* find a solution of the stress balance equations subject to parameterized boundary conditions. The boundary condition parameters are then adjusted so that the sum of that boundary stress solution and the GPE solution conforms to the style of deformation measured in southwestern United States (i.e., the calculated principal stress axes are coaxial with the observed principal strain rate axes, and the ratio of the calculated principal stress deviators is similar to the ratio of observed principal strain rates everywhere). The solution imposed by the adjusted boundary stress [*Flesch et al.*, 2000, Figure 2b] is found to consist of roughly equal parts of north-south compression and east-west extension (i.e., right-lateral shear across vertical planes tangent to the strike of the tangent to the local small circle drawn about the Pacific-NA pole), consistent with the expectation of a shear stress across the transform plate boundary. The east-west spreading observed across most of Nevada (Table 1) is a consequence of the boundary-imposed stress canceling the north-south uniaxial deviatoric tension from the GPE solution, leaving simply the uniaxial east-west deviatoric tension from the boundary-induced stress field. Thus in the formulation of *Flesch et al.* [2000] the boundary-imposed stress field is the primary source of the observed east-west uniaxial deviatoric tension across Nevada.

[28] The stress field of *Flesch et al.* [2000, Figure 2c or 3] is designed to fit a velocity field [*Flesch et al.*, 2000, Figure 1] that in Nevada was deduced principally from earlier GPS surveys [*Thatcher et al.*, 1999, *Bennett et al.*, 1999]. *Flesch et al.* [2000, Figure 3d] have calculated the smoothed velocity field consistent with their stress calculations. Thus a comparison of their stress rates with our measured strain rates amounts to a comparison of their smoothed velocity field [*Flesch et al.*, 2000, Figure 2d] with our more detailed local velocity measurements (Figure 1). The principal difference in this comparison is that the velocity vectors of *Flesch et al.* [2000, Figure 2d] appear to be directed somewhat more northerly than our own.

7.2. Walker Lane Belt

[29] Seismicity in the Walker Lane belt is distributed over many faults [*dePolo et al.*, 1997], and presumably deformation is similarly distributed. Faults within the Walker Lane belt between 39°N and 40°N (Figure 1) are mostly north striking normal faults and northwest striking right-lateral faults; no one dominant fault system cuts through the entire section. The Genoa fault (extending south from Carson City in Figure 1) has a secular normal slip rate of 2–3 mm yr⁻¹ and has produced $M > 7$ earthquakes in the past

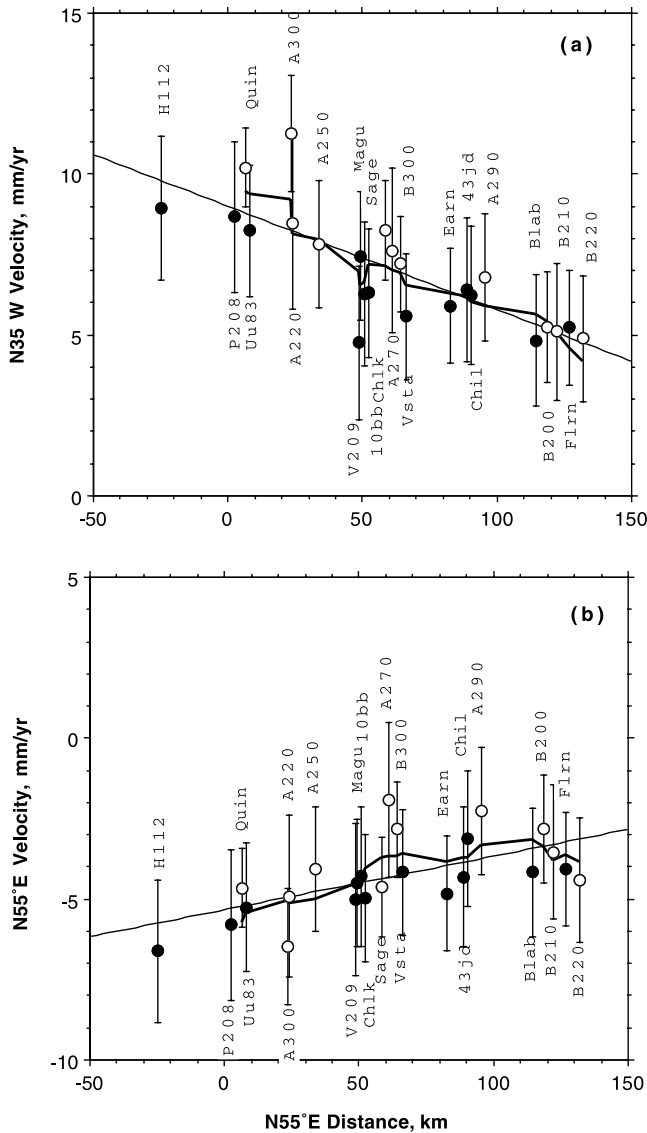


Figure 6. Velocities measured at each monument within the Walker Lane belt plotted as a function of the distance N55°E from a point 10 km west of monument Uu83. Monuments in the Traverse subarray and Quin are identified by open circles, and monuments in the Reno subarray are shown by the solid circles. (a) N35°W velocity and (b) N55°E velocity. The error bars represent 2 standard deviations on either side of the plotted points. Also shown in each plot (solid sinuous line) is a five-point running average of the data and a linear fit (diagonal line).

[Ramelli *et al.*, 1999]. The Pyramid Lake fault zone (extending to the northwest between Fernley and Pyramid Lake) may have been the site of a $M \sim 7$ earthquake in ~ 1850 [Bell and Slemmons, 1979] or 1860 [dePolo *et al.*, 1997] and has certainly been the site of $M > 6.5$ earthquakes in the past [Anderson and Hawkins, 1984]. Stewart [1988] and Cashman and Fontaine [2000] have emphasized the possible importance of northeast striking, left-lateral fault zones (the Olinghouse fault zone, the Carson lineament, and the Wabuska lineament) in this section of the Walker Lane belt. The Olinghouse fault (beneath the label Earn in Figure 1) has been the site of an $M \sim 7$ earthquake in the recent past [Sanders and Slemmons, 1979, 1996], possibly in 1869, though Topozada *et al.* [1981] argue that the epicenter for that earthquake was farther south.

[30] The strain rate field for the Walker Lane belt between 39° and 40°N is given in Table 2. In a coordinate system with the 1' axis directed N55°E and the 2' axis N35°W that strain rate field takes the form

$$\begin{pmatrix} \epsilon'_{11} & \epsilon'_{12} \\ \epsilon'_{12} & 0 \end{pmatrix} \quad (1)$$

where $\epsilon'_{11} = 16.8 \pm 4.9$ nanostrain yr^{-1} , $\epsilon'_{12} = -19.5 \pm 4.0$ nanostrain yr^{-1} , and $\epsilon'_{22} = 0.0 \pm 6.4$ nanostrain yr^{-1} . Notice that within the uncertainties, $\epsilon'_{22} = 0$ and $\omega_r (-13.6 \pm 4.0 \text{ nrad } \text{yr}^{-1})$ is equal to ϵ'_{12} . Thus the motion in the Walker Lane belt is described by right-lateral, simple shear at the rate of ~ 16.6 nstrain yr^{-1} (average of ϵ'_{12} and ω_r) across a vertical plane striking N35°W plus a uniform orthogonal (N55°E) extension at the rate $\epsilon'_{11} = 16.8 \pm 4.9$ nanostrain yr^{-1} with no significant extension along strike. The strike of the tangent to the local small circle drawn about the Pacific-NA pole of rotation [Demets and Dixon, 1999] is also N35°W. That coincidence suggests that the strike-slip component of motion along the zone is driven by the motion of the Pacific plate relative to NA at the plate boundary. The observed extension perpendicular to the zone might be attributed to the high elevation of the NA plate on one side of the plate boundary and the low elevation of the Pacific basin on the other, although the more detailed GPE stress solution of Flesch *et al.* [2000, Figure 2a] suggests otherwise. The stress model of Flesch *et al.* [2000, Figure 2c] predicts uniaxial west-northwest tension in this section of the Walker Lane belt, which is somewhat more northerly than the principal extension direction ($S88.4^\circ W \pm 5.4^\circ$) found for the Walker Lane belt (Table 2).

[31] In 1994, 1996, and 1999, Oldow *et al.* [2001] measured the relative motions within a 50-monument GPS array along the Walker Lane belt between 37.8° to 39.3°N. Their velocity field [Oldow *et al.*, 2001, Figure 3] appears to be similar to ours (Figure 1) where the arrays overlap, but comparison is difficult because the two velocity fields are not referred to the same reference frame. The overall deformation of their network appears to correspond to right-lateral, simple shear across the Walker Lane belt, but Oldow *et al.* [2001] recognize distinct block motions within their velocity field, particularly south of 39°N. We have tentatively identified two such block boundaries in our data: As mentioned in section 3, the anomalous eastward velocities (Figure 3) of monuments H112, P208, and A300 may indicate a block boundary along the Genoa fault, and as shown in Figure 4a, there is a strike-slip boundary along the Fairview Peak fault.

[32] The relatively uniform trend in the north component of velocity plotted as a function of distance east for the Walker Lane belt (west of the vertical line at 160 km in Figure 3a) is a consequence of rotation not shear. North and east correspond closely to the directions of the principal strain rate axes for the strain rate solution for the Walker Lane belt in Table 2. Let u be the east velocity component and v be the north component of velocity. Then $\omega_r = (\partial v/\partial x - \partial u/\partial y)/2$ and $\epsilon_{12} = (\partial v/\partial x + \partial u/\partial y)/2$. It follows that $\partial v/\partial x = \omega_r + \epsilon_{12}$. For the Walker Lane belt subarray, $\epsilon_{12} = 1.2 \pm 4.0$ nstrain yr^{-1} (Table 2), not significantly different from 0. Thus $\partial v/\partial x = \omega_r$, and consequently, the slope of the data exhibited in Figure 3a should be interpreted as a consequence of rigid-body rotation ω_r not deformation (shear rate ϵ_{12}). The slope $\partial u/\partial x$ in Figure 3b is a consequence of deformation (strain rate ϵ_{11}).

[33] Recall that the motion within the Walker Lane belt could be described as simple shear across a zone striking N35°W plus extension perpendicular to that zone. Figure 6 shows a plot of the velocities for the monuments within the Walker Lane belt in a coordinate system in which the 1' axis strikes N55°E and the 2' axis strikes N35°W. Within the precision of measurement, the velocities u' and v' in the Walker Lane belt depend only upon x' because $\epsilon'_{12} = \omega_r$ and $\epsilon'_{22} = 0$: From the relations $\omega_r = (\partial v'/\partial x' -$

$\partial u'/\partial y'/2$ and $\epsilon'_{12} = (\partial v'/\partial x' + \partial u'/\partial y')/2$ given above, $\partial u'/\partial y' = \epsilon'_{12} - \omega_r$. Because $\epsilon'_{12} = \omega_r$, $\partial u'/\partial y' = 0$. Moreover, $\partial v'/\partial y' = 0$ follows from $\epsilon'_{22} = 0$. Thus in Figure 6 the error in projecting velocities onto the N55°E axis is minimized because neither u' nor v' vary with y' . The data in Figure 6, all within the Walker Lane belt, define reasonably uniform trends (diagonal straight lines in Figure 6), demonstrating that the uniform strain in Table 2 is an appropriate approximation.

7.3. CNSZ

[34] Deformation in the CNSZ is controlled by the subparallel north-northeast striking faults shown on the right-hand side of Figure 1. In July and August 1954, rupture occurred along the Rainbow Mountain fault (west of monuments Bora and B230), and in December 1954, rupture occurred along the Fairview Peak (extending from near monument Slr1 to Wond) and Dixie Valley (west of monuments 3756 and B387) faults [Hodgkinson *et al.*, 1996]. In 1932 the Cedar Mountain rupture extended south from near monument Post, and in 1915 the Pleasant Valley rupture extended northward from near monument Mcoy [Goter *et al.*, 1994].

[35] The strain rate for the CNSZ is best described in Table 2 (East Half subarray). That strain rate can also be rotated into the form of equation (1), in which there is no extension along the $2'$ axis. The required rotation is 11.6° clockwise so that the $1'$ axis strikes S78.4°E and the $2'$ axis N11.6°E. In that coordinate system the strain rates are $\epsilon'_{11} = 32.6 \pm 11.0$ nstrain yr⁻¹, $\epsilon'_{12} = -25.1 \pm 6.3$ nstrain yr⁻¹, and $\epsilon'_{22} = 0.0 \pm 5.8$ nstrain yr⁻¹. The rotation rate $\omega_r = -20.3 \pm 6.3$ nrad yr⁻¹ (Table 2) does not differ significantly from the shear strain rate ϵ'_{12} , and the motion of the Fairview array can be interpreted as right-lateral, simple shear across a zone striking N12°E, extension perpendicular to the zone, and no extension parallel to it. The strike of the zone is in good agreement with the average strike (~N10°E) of the Rainbow Mountain, Fairview Peak, and Dixie Valley faults, and the observed motion is consistent with the right-lateral, normal slip on those faults observed in 1954 [Hodgkinson *et al.*, 1996].

[36] The rigid-body motion of the East Half subarray is represented by the Euler vector given in Table 3. The pole of rotation is ~120 km north of Lovelock (Figure 1), and the rotation rate is 1.16° Myr⁻¹ (20 nrad yr⁻¹). We presume that the accumulating strain in the CNSZ will ultimately be released in subsequent earthquakes. The along-strike component of slip in those earthquakes will then release the accumulated right-lateral simple shear across the N12°E striking zone, which will cancel the accumulated rotation. Thus no secular accumulation of rotation is anticipated in the CNSZ.

[37] There is an indication in Figure 4a that right-lateral shear across the Fairview Peak fault may be concentrated close to the 1954 rupture, but the data are not precise enough to exclude the possibility that deformation is uniformly distributed across the CNSZ. The argument for the concentration of shear strain on the fault rupture is based on the offset in the smoothed (five-point running average) curve through the data in Figure 4a. That smoothed curve locates the offset in the velocity profile at the 1954 rupture. It is this coincidence of the offset with the trace of the 1954 rupture that argues most strongly that the offset is real. Indeed, the right-lateral shear in Figure 4a is so abrupt that it might indicate creep on the rupture or perhaps a low elastic modulus fault zone. Alternatively, concentration of strain accumulation close to the fault might be associated with postearthquake relaxation [Thatcher, 1983]. In that case, strain accumulation later in the seismic cycle will be more broadly distributed.

[38] The stress model of Flesch *et al.* [2000, Figure 2c] predicts uniaxial west-northwest deviatoric tension in the CNSZ, whereas the observed principal strain rates for the CNSZ (East Half, Table 2) indicate N49.9°W \pm 6.0° extension (46.2 ± 11.0 nstrain yr⁻¹) and

N40.1°E \pm 6.0° contraction (-13.6 ± 6.1 nstrain yr⁻¹). There is about a 20° discrepancy between the predicted direction of principal tension and the observed direction of principal extension. Moreover, the predicted direction of principal tension (west-northwest) is almost perpendicular to the strike (~N10°E) of the Rainbow Mountain, Fairview Peak, and Dixie Valley faults, all of which exhibited comparable components of right-lateral slip and normal slip in the 1954 ruptures [Hodgkinson *et al.*, 1996]. Because the principal axes of the local stress field associated with the plate boundary conditions [Flesch *et al.*, 2000, Figure 2b] are directed roughly parallel and perpendicular to the strike of the faults in the CNSZ, that stress field is unlikely to drive right-lateral slip on those faults. Thus the right-lateral slip apparently is driven by the GPE stress field, which suggests that the deviatoric tension axis for that field be directed somewhat more westerly than the north-south direction shown by Flesch *et al.* [2000, Figure 2a]. However, the solution of Flesch *et al.* [2000] was intended to describe the generalized stress field in southwestern United States, and one should not expect detailed fits to local situations.

8. Conclusions

[39] Motion in the Walker Lane belt has been described as the deformation of a roughly parallel-sided zone of width ~100 km, striking N35°W (parallel to the tangent to the local small circle drawn about the Pacific-NA pole of rotation), and subject to ~20 nstrain yr⁻¹ right-lateral simple shear across it, ~17 nstrain yr⁻¹ extension perpendicular to it, and no significant extension along it. The right-lateral, simple shear is presumably a consequence of the shear applied at the Pacific-NA plate boundary, and the extension perpendicular to the zone might be imposed by the elevation difference between the Basin and Range province and the Pacific basin. However, Flesch *et al.* [2000, Figure 2a] predict that the GPE-imposed stress is a uniaxial north-northwest deviatoric tension directed not perpendicular (S55°W) to the plate boundary but rather more nearly parallel to it. The superposition of the plate-boundary-imposed stress field causes the principal strain rates (29.6 \pm 5.3 nstrain yr⁻¹ S88.4°W \pm 5.4° and -12.8 ± 6.0 nstrain yr⁻¹ N01.6°W \pm 5.4°) observed within the Walker Lane belt to be reasonably consistent with the uniaxial west-northwest tension predicted by Flesch *et al.* [2000, Figure 2c].

[40] Motion in the CNSZ (East Half array) can be described by the deformation of a parallel-sided zone of width ~75 km, striking N12°E (parallel to the principal faults within the zone), and subject to ~25 nstrain yr⁻¹ right-lateral simple shear across it, ~33 nstrain yr⁻¹ extension perpendicular to it, and no significant extension along it. The principal strain rates (46.2 ± 11.0 nstrain yr⁻¹ N49.9°W \pm 6.0° and -20.3 ± 6.3 nstrain yr⁻¹ N40.1°W \pm 6.0°) observed near the CNSZ are not completely consistent with the uniaxial west-northwest deviatoric tension predicted by Flesch *et al.* [2000, Figure 2c]; the principal tension axis should be directed more northerly. The strain rate field here is clearly associated with the principal faults (Rainbow Mountain, Fairview Peak, and Dixie Valley faults) in the CNSZ and could be attributed to slip at depth on those faults. That is, the regional stress field probably has been distorted in the vicinity of the CNSZ due to the presence of active faults (flaws in the lithosphere). Nevertheless, the regional stress field must be oriented so that when resolved onto the fault surface it will drive right-lateral, normal slip. The uniaxial west-northwest tension found by Flesch *et al.* [2000, Figure 2c] is not well oriented to accomplish this.

Appendix A: Simple Shear

[41] Consider the surface deformation at a shear zone. Choose the y axis parallel to the shear zone, the x axis perpendicular to it,

and the origin within the zone. Assume that the strain rate ε_{12} and rotation rate ω_r are uniform within the zone and that the only nonzero component of the strain rate is ε_{12} . The velocity relative to the origin of a point within the shear zone is [Jaeger, 1964, p. 39]

$$u = (\varepsilon_{12} - \omega_r)y, \quad (A1)$$

$$v = (\varepsilon_{12} + \omega_r)x. \quad (A2)$$

We now consider pure shear and simple shear [Jaeger, 1964, p. 24]. In the absence of any rotation ω_r we have pure shear. Simple shear parallel to the y axis corresponds to $\varepsilon_{12} = \omega_r$ in which case $u = 0$, $v = 2\varepsilon_{12}x$, and the velocity is parallel to the y axis as required. Simple shear parallel to the x axis corresponds to $\varepsilon_{12} = -\omega_r$ in which case $u = 2\varepsilon_{12}y$, $v = 0$, and the velocity is parallel to the x axis as required. Clearly, simple shear parallel to the x axis can be converted to simple shear parallel to the y axis by simply adding a rotation $2\varepsilon_{12}$.

[42] **Acknowledgments.** We thank Geoffrey Blewitt for a constructive review of an earlier version of this paper.

References

- Anderson, L. W., and F. F. Hawkins, Recurrent Holocene strike-slip faulting, Pyramid Lake fault zone, western Nevada, *Geology*, *12*, 681–684, 1984.
- Bell, E. J., and D. B. Slemmons, Recent crustal movements in the central Sierra Nevada Walker Lane region of California-Nevada, part II, The Pyramid Lake right-slip fault zone segment of the Walker Lane, *Tectonophysics*, *52*, 571–583, 1979.
- Bennett, R. A., J. L. Davis, and B. P. Wernicke, Present-day pattern of Cordilleran deformation in the western United States, *Geology*, *27*, 371–374, 1999.
- Bomford, G., *Geodesy*, 3d ed., 731 pp., Clarendon, Oxford, England, 1971.
- Cashman, P. H., and S. A. Fontaine, Strain partitioning in the northern Walker Lane, western Nevada and northeastern California, *Tectonophysics*, *326*, 111–130, 2000.
- Caskey, S. J., S. G. Wesnousky, P. Zhang, and D. B. Slemmons, Surface faulting of the 1954 Fairview Peak (M_s 7.2) and Dixie Valley (M_s 6.8) earthquakes, central Nevada, *Bull. Seismol. Soc. Am.*, *86*, 761–787, 1996.
- Demets, C., and T. H. Dixon, New kinematic models for Pacific-North America motion from 3 Ma to present, I, Evidence for steady motion and biases in the NUVEL-1A model, *Geophys. Res. Lett.*, *26*, 1921–1924, 1999.
- dePolo, C. M., J. G. Anderson, D. M. dePolo, and J. G. Price, Earthquake occurrence in the Reno-Carson City urban corridor, *Seismol. Res. Lett.*, *68*, 401–412, 1997.
- Dixon, T. H., M. Miller, F. Farina, H. Wang, and D. Johnson, Present-day motion of the Sierra Nevada block and some tectonic implications for the Basin and Range province, North America Cordillera, *Tectonics*, *19*, 1–24, 2000.
- Dong, D., T. A. Herring, and R. W. King, Estimating regional deformation from a combination of space and terrestrial geodetic data, *J. Geod.*, *72*, 200–214, 1998.
- England, P., and J. Jackson, Active deformation of the continents, *Annu. Rev. Earth Planet. Sci.*, *17*, 197–226, 1989.
- Flesch, L. M., W. E. Holt, A. J. Haines, and B. Shen-Tu, The dynamics of the Pacific-North America plate boundary zone in the western United States, *Science*, *287*, 834–836, 2000.
- Goter, S. K., D. H. Oppenheimer, J. Mori, M. K. Savage, and R. P. Masse, Earthquakes in California and Nevada (map), *U.S. Geol. Surv. Open File Rep.*, 94-647, 1994.
- Hodgkinson, K. M., R. S. Stein, and G. Marshall, Geometry of the 1954 Fairview Peak-Dixie Valley earthquake sequence from a joint inversion of leveling and triangulation data, *J. Geophys. Res.*, *101*, 25,437–25,457, 1996.
- Jaeger, J. C., *Elasticity, Fracture and Flow*, 212 pp., Methuen, New York, 1964.
- Jennings, C. W., Fault activity map of California and adjacent areas, *Geol. Data Map 6*, Calif. Div. of Mines and Geol., Dep. of Conserv., Sacramento, 1994.
- Jones, C. H., J. R. Unruh, and L. J. Sonder, The role of gravitational potential energy in active deformation in the southwestern United States, *Nature*, *381*, 37–41, 1996.
- Oldow, J. S., C. L. V. Aiken, J. L. Hare, J. F. Furguson, and R. F. Hardyman, Active displacement transfer and differential block motion within the central Walker Lane, western Great Basin, *Geology*, *29*, 19–22, 2001.
- Pezzopane, S. K., and R. J. Weldon, Tectonic role of active faulting in central Oregon, *Tectonics*, *12*, 1140–1169, 1993.
- Ramelli, A. R., J. W. Bell, C. M. dePolo, and J. C. Yount, Large-magnitude, late Holocene earthquakes on the Genoa fault, west central Nevada and eastern California, *Bull. Seismol. Soc. Am.*, *89*, 1458–1472, 1999.
- Sanders, C. O., and D. B. Slemmons, Recent crustal movements in the central Sierra Nevada-Walker Lane region of California-Nevada, part III, The Olinghouse fault zone, *Tectonophysics*, *52*, 585–597, 1979.
- Sanders, C. O., and D. B. Slemmons, Geomorphic evidence for Holocene earthquakes in the Olinghouse fault zone, western Nevada, *Bull. Seismol. Soc. Am.*, *86*, 1784–1792, 1996.
- Savage, J. C., M. Lisowski, J. L. Svarc, and W. K. Gross, Strain accumulation across the central Nevada seismic zone, *J. Geophys. Res.*, *100*, 20,257–20,269, 1995.
- Savage, J. C., W. Gan, and J. L. Svarc, Strain accumulation and rotation in the Eastern California Shear Zone, *J. Geophys. Res.*, *106*, 21,995–22,007, 2001.
- Sillard, P., Z. Altamimi, and C. Boucher, The ITRF96 realization and its associated velocity field, *Geophys. Res. Lett.*, *25*, 3223–3226, 1998.
- Slemmons, D. B., D. van Wormer, E. J. Bell, and M. L. Silberman, Recent crustal movements in the central Sierra Nevada-Walker Lane region of California-Nevada, part I, Rate and style of deformation, *Tectonophysics*, *52*, 561–570, 1979.
- Stewart, J. H., Tectonics of the Walker Lane Belt, western Great Basin: Mesozoic and Cenozoic deformation in a zone of shear, in *Metamorphism and Crustal Evolution of the Western United States*, Rubey vol. VII, edited by W. G. Ernst, pp. 683–713, Prentice-Hall, Old Tappan, N. J., 1988.
- Svarc, J. L., J. C. Savage, W. H. Prescott, and M. H. Murray, Strain accumulation and rotation in western Oregon and southwestern Washington, *J. Geophys. Res.*, *107*(B5), 10.1029/2001JB000625, 2002.
- Thatcher, W., Nonlinear strain buildup and the earthquake cycle on the San Andreas fault, *J. Geophys. Res.*, *88*, 5893–5902, 1983.
- Thatcher, W., G. R. Foulger, B. R. Julian, J. Svarc, E. Quilty, and G. W. Bawden, Present-day deformation across the Basin and Range province, western United States, *Science*, *283*, 1714–1718, 1999.
- Topozada, T. R., C. R. Real, and D. L. Parke, Preparation of isoseismal maps and summaries of reported effects for pre-1900 California earthquakes, *Calif. Div. Mines Geol. Open File Rep.*, 81-11SAC, 182 pp., 1981.
- Webb, F. H., and J. F. Zumberge, *An Introduction to GIPSY/OASIS-II*, JPL D-11088, Jet Propul. Lab., Calif. Inst. of Technol., Pasadena, 1995.
- Weertman, J., Deformation of floating ice shelves, *J. Glaciol.*, *3*, 38–42, 1957.
- Wernicke, B., A. M. Friedrich, N. A. Niemi, R. A. Bennett, and J. L. Davis, Dynamics of plate boundary fault system from Basin and Range geodetic network (BARGEN) and geologic data, *GSA Today*, *10*, 1–7, 2000.
- Zumberge, J. F., M. B. Heflin, D. C. Jefferson, M. M. Watkins, and F. H. Webb, Precise point positioning for the efficient and robust analysis of GPS data from large networks, *J. Geophys. Res.*, *102*, 5005–5017, 1997.

W. H. Prescott, J. C. Savage, and J. L. Svarc, U.S. Geological Survey, MS/977, 345 Middlefield Road, Menlo Park, CA 94025, USA. (wprescott@usgs.gov; jasavage@usgs.gov; jsvarc@usgs.gov)

A. R. Ramelli, Nevada Bureau of Mines and Geology, University of Nevada, MS 178, Reno, NV 89557, USA. (ramelli@unr.edu)